Experimental studies of fast electron generation in laser-produced plasmas at 1.06, 0.53 and 0.26 μm laser wavelength

François Amiranoff, R. Fabbro, E. Fabre, C. Garban-Labaune, M. Weinfeld

J. Physique **43** (1982) 1037-1042 JUILLET **1982,** PAGE 1037

Classification
Physics Abstracts
52.50J

Experimental studies of fast electron generation in laser-produced plasmas at 1.06, 0.53 and 0.26 μm laser wavelength (*)

F. Amiranoff, R. Fabbro, E. Fabre, C. Garban-Labaune and M. Weinfeld

Laboratoire P.M.I., Groupe de Recherche N° 29 du C.N.R.S.,
Ecole Polytechnique, 91128 Palaiseau Cedex, France

(*Reçu le 8 janvier 1982, accepté le 15 mars 1982*)

Résumé. — Nous présentons des résultats expérimentaux sur la génération des électrons rapides dans les plasmas créés par laser à 1,06, 0,53 et 0,26 μm à des flux compris entre 10^{14} et 2×10^{15} W/cm^2. Les mesures du rayonnement X et de collecteurs d'ions indiquent une température chaude donnée par

$$T_H \simeq 4 \times 10^{-7} (I\lambda^2/\mathrm{W.\mu m^2.cm^{-2}})^{0,5} \text{ keV}.$$

Abstract. — We present experimental results on fast electron generation in laser-produced plasmas at 1.06, 0.53 and 0.26 μm at laser intensities between 10^{14} and 2×10^{15} W/cm^2. Hard X-ray and ion-collector data are in good agreement and indicate a hot temperature given by $T_H = 4 \times 10^{-7}$ $(I\lambda^2/\mathrm{W.\mu m^2.cm^{-2}})^{0.5}$ keV.

1. **Introduction.** — At large laser intensities a large fraction of the absorbed energy can be transferred in the plasma to a small number of electrons accelerated by electrostatic waves due to resonance absorption [1, 2] or parametric instabilities [3]. These electrons can reach a typical energy of several tens of keV and are able to penetrate deeply in solid material, giving rise to some pusher and target core preheating and impairing the achievement of ablative compressions.

Numerical simulations of hot electron generation by resonance absorption [1, 2] predict an important decrease of their average energy when using short wavelength lasers. Many experimental results on X-ray spectra have been obtained in different laboratories at 1.06 [4-10], 10.6 [8, 11-13] and 0.69 [14] μm laser wavelengths. A part of the results presented below and some other work have already been published for shorter wavelengths [9, 10]. We present our results on hot electron generation at different laser wavelengths (1.06, 0.53 and 0.26 μm) and different pulse durations (100 ps, 2.5 ns) at intensities between 10^{14} and 2×10^{15} W/cm^2 on massive plastic targets. The results of absorption measurements in the same conditions are presented elsewhere [15]. The diagnostics used in this experiment are an X-ray multichannel analyser between 1 and 70 keV and ion charge collectors.

2. **Experimental set-up.** — The Nd glass laser of the G.I.L.M. at Palaiseau was used in short pulse (100 ps FWHM) or long pulse (2.5 ns) regime. The 90 mm diameter output beam of maximum energy at 1.06 μm, 10 J in short pulse and 50 J in long pulse is frequency doubled with a first KDP crystal to make experiments at 0.53 μm. A second KDP crystal provides a 0.26 μm laser beam. The beam — 1.06, 0.53 or 0.26 μm — is then focussed at normal incidence onto plane plastic targets ($C_{10}H_8O_4$) with a $f/1.3$ lens in each case.

To keep the geometry of the interaction constant when changing the incident flux we always put the target at the same position defined as the position where the maximum hard X-ray emission occurs. The diameter of the focal spot is measured by the burn paper method. The characteristics of the different beams are summarized in table I.

The two diagnostics used are a continuum X-ray multi-channel analyser and charge collectors located in front of the target to detect the fast ion emission. The 10 X-ray channels based on the absorbing foil method [16] are listed in table II. Magnets located in front of the p.i.n. diodes used as soft X-ray detectors protect them against fast electrons hitting directly the diode or causing some fluorescence in the filter.

(*) This work is part of the GRECO ILM scientific program.

Table I. — *Different experimental conditions.*

Wavelength	Pulse Duration	Aperture	Focal spot size (FWHE)	Maximum flux
1.06 μm	100 ps	$f/1.3$	60 ± 15 μm	2×10^{15} W/cm^2
1.06 μm	2.5 ns	$f/1.3$	60 ± 15 μm	4×10^{14} W/cm^2
0.53 μm	80 ps	$f/1.3$	50 ± 15 μm	10^{15} W/cm^2
0.53 μm	2 ns	$f/1.3$	50 ± 15 μm	4×10^{14} W/cm^2
0.27 μm	60 ps	$f/1.3$	70 ± 20 μm	4×10^{14} W/cm^2

Table II. — *Characteristics of the different X-ray channels.*

N°	Absorber	Detector	Mean energy (keV)
1	Be 25 μm	p.i.n. diode	1-1.5
2	Be 125 μm	—	1.4-2.1
3	Ti 20 μm	—	3-5
4	Fe 25 μm	—	5-7.1
5	Ni 25 μm	—	6-8.3
6	Zn 50 μm	—	7-9.7
7	Al 500 μm	NaI 1 mm	10-20
8	Mo 100 μm	—	12-20
9	Sn 250 μm	—	20-29
10	Ta 500 μm	—	50-67

p.i.n. diode from Quantrad, 250 μm of silicium.

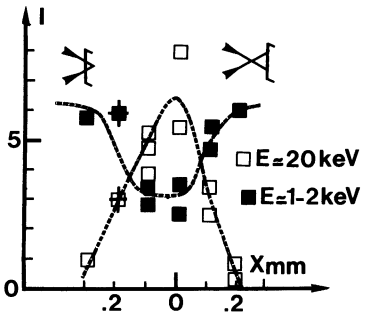

Fig. 1. — Soft (1-2 keV) and hard (20 keV) signal *versus* target position. $\lambda = 1.06$ μm; $\tau = 100$ ps. The dotted lines follow the mean values of the data. Crosses are the error bars for each shot.

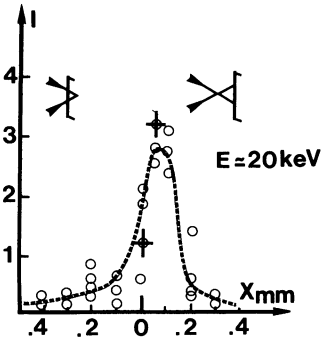

Fig. 2. — Hard X-ray signal (20 keV) *versus* target position. $\lambda = 1.06$ μm; $\tau = 2.5$ ns. The dotted line follows the mean values of the data. Crosses are the error bars for each shot.

The constant 4 cm long 700 G magnetic field is sufficient to stop most electrons. Hard X-rays are detected by NaI scintillators coupled with 56 TVP photomultiplier tubes. A thick lead protection ($\sim$ 1 cm) is used against any noise coming from the target chamber. The calibration of these detectors using Cd and Am radioactive sources is known within 50 % error bars. The hard X-ray detectors give us information on fast electrons produced in the plasma and radiating in high density regions. Energy exchange between fast electrons and ions in the corona is studied with ion charge collectors protected against secondary emission and located 40 cm in front of the target normal. To obtain a hot electron temperature, the deconvolution of the signals is performed with the assumption of a two temperature isothermal expansion [17].

3. **Experimental results.** — The analysis of the X-ray spectrum was made at focussing conditions corresponding to the maximum hard X-ray emission. The analysis of the X-ray intensity dependence with target position shows that the maximum is obtained nearly at focus within 30 μm. This was also a reason for us to use this technique as a focal spot determination.

The intensity of a hard X-ray channel ($E \simeq 20$ keV) is plotted *versus* the target position on figures 1 and 2 respectively for short and long pulses at 1.06 μm. As seen on figure 1 the sharp maximum of the hard X-ray signal corresponds to a dip of the soft X-rays not correlated with a decrease of the absorption [15]. A clear understanding of this dip appearing only with short pulse at 1.06 μm cannot be given at present. We think that it depends on detailed variations of the focal spot and the resulting plasma temperature. The strong modification of longitudinal transport due to large fast electrons lateral transport may also play a role.

The same evolution is observed for the ionic emission. The quantity of fast and slow ions received by a charge collector 30° from the target normal is plotted

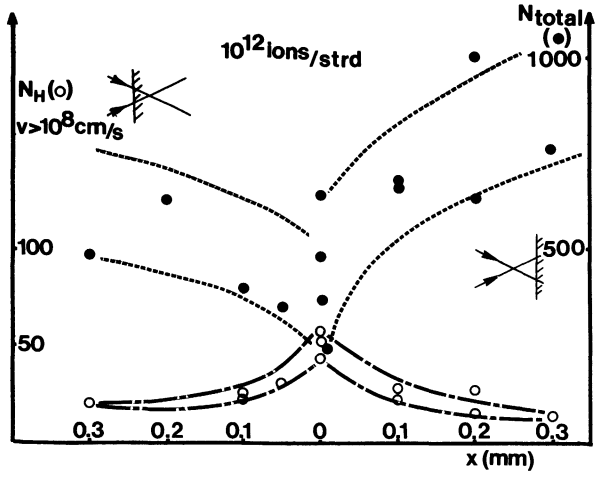

Fig. 3. — Number of slow and fast ions ($v > 10^8$ cm/s) *versus* target position. $\lambda = 1.06$ μm; $\tau = 100$ ps. The dotted lines are shot to shot scattering limits.

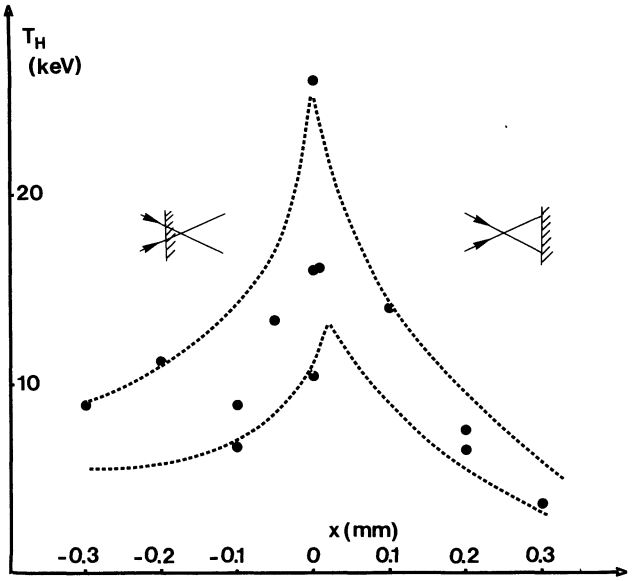

Fig. 4. — Hot electron temperature deduced from the fast ion signal *versus* target position. $\lambda = 1.06$ μm; $\tau = 100$ ps. The dotted lines are shot to shot scattering limits.

versus the focal position in figure 3. The hot electron temperature deduced from those fast ion signals is plotted in figure 4.

The hot electron temperature determination is also performed through analysis of hard X-ray spectra at different intensities and wavelengths. Because the hard X-ray amplitude decreases very rapidly at low flux or short wavelength, the temperature is deduced from the slope of the spectrum between 15 and 60 keV at 1.06 μm and intensities greater than 5×10^{14} W/cm^2, between 15 and 40 keV for lower intensities and for $\lambda = 0.53$ μm. At $\lambda = 0.26$ μm, the last useful channel being the seventh ($E \simeq 15$ keV), the result was correlated with results given by another method described later. Figure 5 summarizes the results.

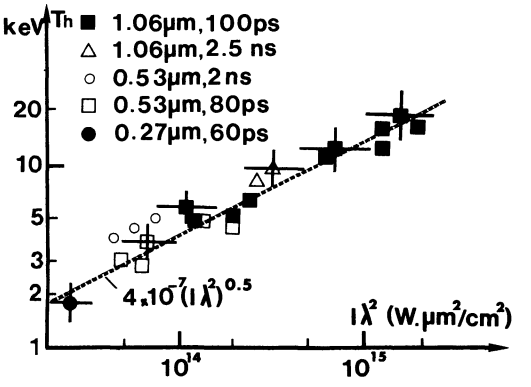

Fig. 5. — Hot electron temperature deduced from hard X-ray spectra *versus* $I\lambda^2$ with typical error bars in each condition.

The three major conclusions are the following :

1) Hot electron temperature is strongly reduced when using low intensities or short wavelengths.

2) The temperature does not seem to depend on the pulse duration. This is probably explained by the fact that absorption, even classical, still takes place near the critical density at 2.5 ns. Consequently the density profile modification will be comparable in long and short pulse regime.

3) An experimental law can be extracted from the results and a good fit to the data of figure 5 is

$$T_H = 4 \times 10^{-7}(I\lambda^2)^{0.5} \text{ keV}$$

with I in W/cm^2 and λ in μm.

Typical spectra obtained at 1.06 μm in short pulse are plotted in figure 6. The slope of the soft part of the spectrum ($E \simeq 1$ to 3 keV) is characteristic of a « temperature » of 300 ± 50 eV which does not depend — or very slowly — on the incident flux.

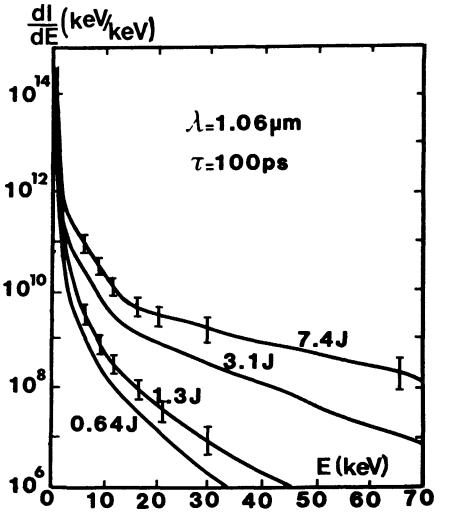

Fig. 6. — Typical X-ray spectra obtained at $\lambda = 1.06$ μm; $\tau = 100$ ps and fluxes of 1.3×10^{14}, 2.6×10^{14}, 6.3×10^{14} and 1.5×10^{15} W/cm^2.

But the spatially integrated soft X-ray signal only provides a « mean temperature of the overcritical region » because of the high dependence of the emission on the local density, as n^2. On the other hand the high energy part of the spectrum is very sensitive to the incident flux due to the important variations of the fast electron temperature.

Figure 7 shows typical spectra obtained in long pulse at 1.06 μm and in short pulse at 0.53 and 0.26 μm. The spectra at shorter wavelengths show a higher soft signal than at 1.06 μm because the hot region at the critical density is at larger densities. The spectrum temperature are 350 ± 50 eV at 0.53 μm and

$$400 \pm 50 \text{ eV at } 0.26\ \mu\text{m}.$$

The high energy part of the spectra clearly shows the decrease of the hot electron temperature at short wavelengths.

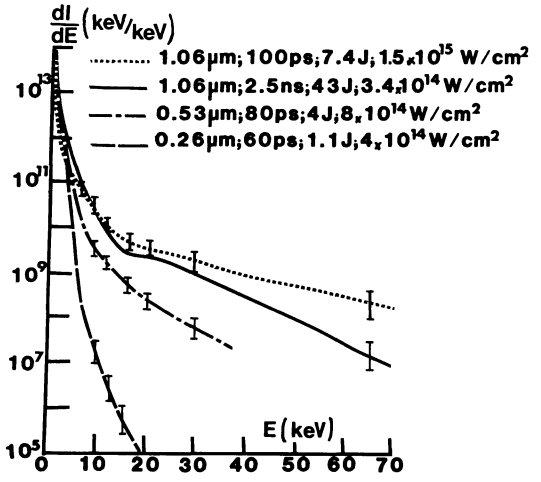

Fig. 7. — Typical X-ray spectra obtained at the three wavelengths.

Showing that the total X-ray emission of a fast electron does not depend on its detailed path in the plasma, Brueckner derives a formula giving the energy in fast electrons from the amount of hard X-rays emitted [18]. From our spectra we find 5 % to 20 % of the absorbed energy in fast electrons using short pulse at 1.06 μm and about 2 % using long pulses. This shows that although the hot electron temperature remains approximately constant, the fraction of energy in fast electrons decreases for longer pulses. The short pulse value at 0.53 μm gives values comparable to the 1.06 μm one : 10 to 20 %.

We must emphasize here that this determination does not take into account the energy lost by fast electrons into the acceleration of ions in the corona so that the indicated values are only a minimum and one should add the energy measured in fast ions to obtain a more accurate estimation of the initial energy in the fast electron population. This point will be discussed later on.

The temperature obtained at $\lambda = 0.26$ μm, difficult to measure directly on the spectrum, has been confirmed by comparing one hard X-ray channel signal [$E \simeq 15$ keV] at different wavelengths. The signal normalized to the incident energy is plotted *versus* $I\lambda^2$ on figure 8. The different curves are theoretical estimates where the X-ray spectrum used to compute the signal of the channel is defined by two conditions. First the temperature (slope) of the spectrum is supposed to follow a law $T_H = a(I\lambda^2)^\alpha$ where a is constant and α is an adjustable parameter.

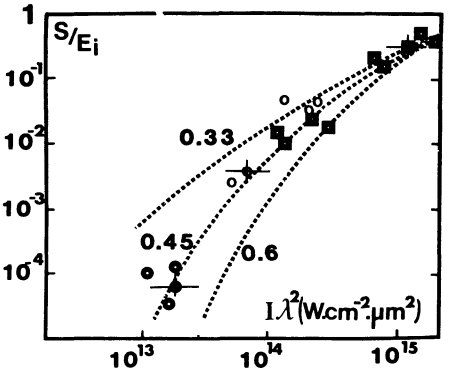

Fig. 8. — Hard X-ray signals $S(E \simeq 15$ keV) normalized to incident energy E_i *versus* $I\lambda^2$. Different theoretical curves are for $T_H = a(I\lambda^2)^\alpha$ for different α.

Secondly its amplitude is fixed by the condition that the energy in the fast electrons emitting this spectrum is the same fraction of the incident energy at the three wavelengths. Taking reference [8], this condition can be expressed as $dE/d(h\nu)(h\nu = T_H) = \text{const.}$ where E is the energy emitted at frequency ν. The spectrum corresponding to a Maxwellian electron distribution and verifying this condition is then

$$dE/d(h\nu) = AT_H^{1/2} \exp[-h\nu/T_H] \times (h\nu)^{-1/2}$$

where A is a constant independent of $I\lambda^2$. Taking for T_H at 1.06 μm the experimental values the first condition determines T_H for any α and $I\lambda^2$. The curves corresponding to different α are given. We can see on figure 8 that the best fit is obtained for $\alpha \simeq 0.45$ — which is the experimental value for 1.06 μm and 0.53 μm (see Fig. 5) — so that for $\lambda = 0.26$ μm and $\phi = 2$ to 4×10^{14} W/cm^2 we have $T_H \simeq 2$ keV. Moreover it is clear on figure 8 where the total variation of the normalized signal is four orders of magnitude, that a change of a factor 2 or 3 in the second condition — allowing for instance less energy in fast electrons at 0.27 μm — would not change very much the best value of α and then the extimated temperature.

These results obtained from X-ray spectra are well correlated with the study of fast ions emitted from the plasma. The deconvolution of charge collector signals with a two-temperature isothermal expansion model gives a hot electron temperature which compares well with the preceding results. Figure 9 shows this compa-

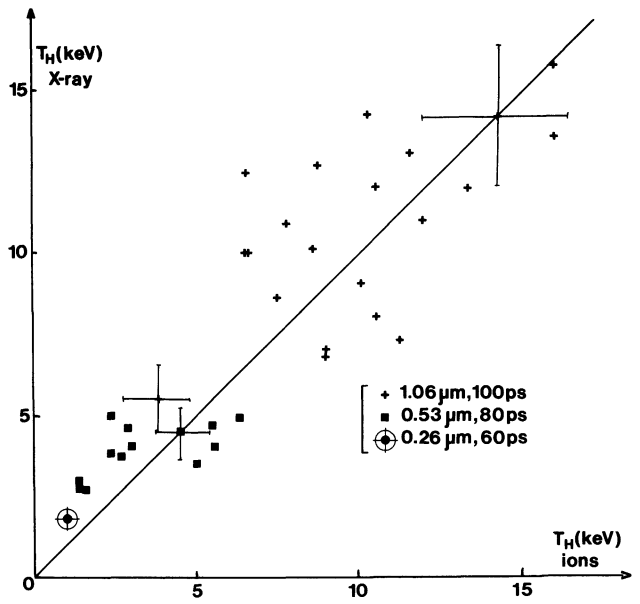

Fig. 9. — Comparison of hot electron temperature deduced from ion and X-ray signals.

rison for different fluxes, wavelengths and pulse durations. The hypothesis made here that fast ions are mainly H^+ certainly reduces the estimated temperature when it is low. In these conditions it seems reasonable to think that they are formed of H^+ and C^{6+} so that the ratio mass/charge is between 1 and 2 thus increasing the estimated values. At high intensities on the other hand, it has been shown that fast ions are mainly H^+ [21].

The ionic distribution functions obtained at the three wavelengths for comparable absorbed fluxes are plotted in figure 10. We can see an important

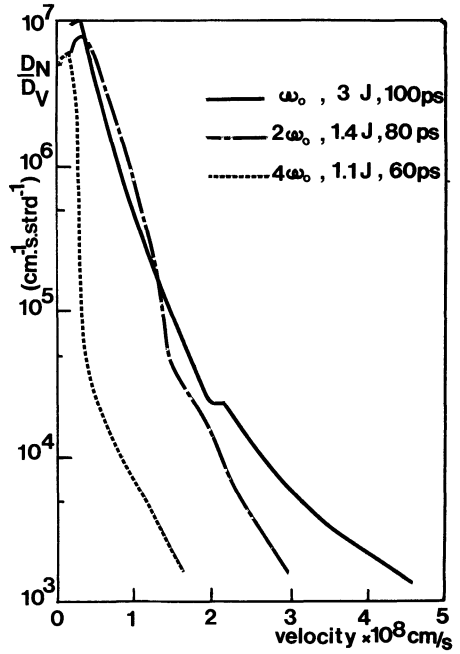

Fig. 10. — Typical ion spectra at the three wavelengths.

decrease of the hot temperature and of the number of fast ions at short wavelengths. The fast ions are defined as those faster than the speed corresponding to the change of the slope in the distribution function.

Preliminary results on the total energy of these fast ions assuming that they are mainly H^+ indicate a fraction of about 20 to 30 % of the absorbed energy at 1.06 μm and 2×10^{15} W/cm^2 (the presence of heavier ions would even increase this fraction). It shows that the total energy in fast electrons — obtained from the X-ray spectra and the fast ions — represent at least at 1.06 μm a large fraction (25 % to 50 %) of the absorbed laser energy.

Measurements of hard X-ray spectra and fast ions emitted from laser-produced plasmas at 1.06, 0.53 and 0.26 μm laser wavelength show that the hot electron temperature is given by

$$T_H \simeq 4 \times 10^{-7} (I\lambda^2/\mathrm{W.cm^{-2}.\mu m^2})^{0.5} \text{ keV} .$$

This result obtained in the range $2 \times 10^{13} \leqslant I\lambda^2 \leqslant 2 \times 10^{15}$ W.cm^{-2}.μm^2 is valid for short or long laser pulses. However if the temperatures are nearly equal in both cases, the experiments exhibit much less hard X-rays and fast ions for long pulses.

These results agree quite well with the previously published data concerning 1.06 μm and 10.6 μm lasers — see for instance figure 4 in [1] and figure 2 in [2] — and concerning 0.53 μm lasers [9]. The measured slopes in [1] and [9], $\alpha = 0.31$-0.39 are obtained at higher intensities, up to 10^{16} W.μm^2.cm^{-2}. In reference [2] a change of the slope from $\alpha = 0.67$ to $\alpha = 0.25$ at about 10^{15} W.μm^2.cm^{-2} is noted. In our case the curve of figure 5 can as well be fitted by a first line of slope $\alpha = 2/3$ and a second portion with $\alpha \simeq 0.4$ at $I\lambda^2 \gtrsim 5 \times 10^{14}$ W.μm^2.cm^{-2}. Experiments at higher intensities could allow to see this effect.

The different theoretical scaling laws for the hot electron temperature are of the form T_H proportional to $(I\lambda^2)^\alpha$. Flux limit arguments when electrons are stochastically heated in the corona predict $\alpha = 2/3$ [19]. Simulations of resonant absorption show two different regimes. In the « cold-dynamics » regime [20] where $v_0/v_e \lesssim 1 - v_0$ is the quiver velocity of an electron in the vacuum laser field and v_e is the thermal electron velocity — α is 2/3 as in the previous case. In the « hot dynamics » regime [1, 2] where $v_0/v_e \gtrsim 1$ the profile modification induced by the laser gives $\alpha = 1/3$ or 2/5.

Here again our measured mean value, $\alpha \simeq 0.5$, is intermediate between these different estimates and high intensity experiments are needed to point out the predicted modification.

We would like to emphasize that the most important result is the wavelength scaling of T_H — proportional to λ — which shows that the use of short wavelength lasers could greatly reduce the problems caused by fast electron preheating and plasma target decoupling in ablative compression experiments. It could simplify

the target design by reducing the amount of high Z material needed for fast electron shielding and open the possibility of using short wavelength lasers at high intensities to drive efficient implosions.

Acknowledgments. — We would like to thank D. Bruneau, C. Loth, A. Michard, J. L. Militon, A. Olmedo, J. M. Saura, H. Timsit and A. M. Tournade for their assistance in all these experiments.

References

[1] ESTABROOK, K. and KRUER, W. L., *Phys. Rev. Lett.* **40** (1978) 42.

[2] FORSLUND, D. W., KINDEL, J. M. and LEE, K., *Phys. Rev. Lett.* **39** (1977) 284.

[3] THOMSON, J. J., FAEHL, R. J. and KRUER, W. L., *Phys. Rev. Lett.* **31** (1973) 918.

[4] SLIVINSKY, V. W., KORNBLUM, H. N., SHAY, H. D., *J. Appl. Opt.* **46** (1975) 1973.
HAAS, R. A. *et al.*, *Phys. Fluids* **20** (1977) 322.

[5] LEE, P. H. and ROSEN, M. D., *Phys. Rev. Lett.* **42** (1979) 236.

[6] BURKHALTER, P. G. *et al.*, *Phys. Rev. A* **15** (1977) 1191.

[7] LUTHER DAVIES, B., *Appl. Phys. Lett.* **32** (1978) 209.

[8] KEPHART, J. F., GODWIN, R. P. and MCCALL, G. H., *Appl. Phys. Lett.* **25** (1974) 108.

[9] SLATER, D. C. *et al.*, *Phys. Rev. Lett.* **46** (1981) 1199.

[10] AMIRANOFF, F., FABBRO, R., FABRE, E., GARBAN, C., VIRMONT, J. and WEINFELD, M., *Phys. Rev. Lett.* **43** (1979) 522.
FABRE, E., AMIRANOFF, F., FABBRO, R., GARBAN-LABAUNE, C., VIRMONT, J., WEINFELD, M., DAVID, F., PELLAT, R., *Plasma physics and controlled nuclear fusion research 1980* (1981) Vol. II, p. 263.

[11] STENZ, C. *et al.*, *J. Physique* **38** (1977) 761.

[12] PEPIN, H., MARTIN, F., GREK, B., JOHNSTON, T. W., KIEFFER, J. C. and MITCHEL, G., *J. Appl. Phys.* **50** (1979) 6784.

[13] ENRIGHT, G. D., RICHARDSON, M. C. and BURNETT, N. H., *J. Appl. Phys.* **50** (1979) 3909.

[14] BLAZHENKOV, V. V. *et al.*, *Phys. Lett.* **78A** (1980) 347.

[15] GARBAN-LABAUNE, C. *et al.*, *GRECO ILM Annual Report 1979* (to be published).

[16] JAHODA, F. C. *et al.*, *Phys. Rev.* **119** (1960) 843.

[17] WICKENS, L. M., ALLEN, J. E., RUMSBY, P. T., *Phys. Rev. Lett.* **41** (1978) 243.

[18] BRUECKNER, K. A., LEE, Y. T., *Nucl. Fusion* **19** (1979) 1431.

[19] MORSE, R. L. and NIELSON, C. W., *Phys. Fluids* **16** (1973) 909.

[20] ALBRITTON, J. R. and LANGDON, A. B., *Phys. Rev. Lett.* **45** (1980) 1794.

[21] WAGLI, P., DONALDSON, T. P. and LADRACH, P., *Appl. Phys. Lett.* **32** (1978) 638.